J. Fluid Mech. (1983), *vol.* 130, *pp.* 219–239
Printed in Great Britain

A class of elliptical free-surface flows

By A. L. NEW†
School of Mathematics, University of Bristol, University Walk, Bristol BS8 1TW, England

(Received 27 August 1982)

Exact solutions of the equations of motion for an inviscid fluid are rare. Using the formalism of John (1953), this paper presents a class of exact zero-gravity flows in which the free surface assumes the form of an ellipse having arbitrary but time-constant aspect ratio. The dynamically important region beneath the overturning crest of a breaking gravity wave is examined and the profile is found to be remarkably well approximated by a $\sqrt{3}$ aspect-ratio ellipse. The range of examples presented includes high-resolution computations in both deep and shallow water, and also the plunger-generated laboratory waves of Miller (1976).

The ellipse solution is shown to model qualitatively certain essential features of the numerical waves. A recent self-similar solution due to Longuet-Higgins (1981, 1982), in which the free surface is a parametric cubic curve, is also discussed.

1. Introduction

As is often remarked, exact time-dependent solutions of the equations of motion for an inviscid fluid with a free surface are quite rare. One classical example is the so-called ellipsoid of Dirichlet (see Lamb 1932, Art. 382) in which the self-gravitating mass of fluid has an ellipsoidal surface. Longuet-Higgins (1972) presents a class of exact free-surface zero-gravity flows related to these ellipsoids, in which the two-dimensional surface may assume the form of either a variable ellipse or hyperbola, or a pair of parallel lines. Generalizations are shown to include the Dirichlet parabola (Longuet-Higgins 1976), and also flows with rotating axes (Longuet-Higgins 1980). (In this latter paper it is suggested that the flow near the tip of a breaking gravity wave may be modelled by a rotating form of the Dirichlet hyperbola.) The rotational gravity wave of Gerstner (see Lamb 1932, Art. 251), and the pure capillary wave of Crapper (1957) are also well-known examples.

In this paper we present an exact free-fall solution to the equations of motion in which the free surface takes the form of an ellipse with a time-constant aspect ratio (being defined as the ratio major axis/minor axis). These flows are hence different in character to the Dirichlet ellipses mentioned above, which instead preserve a constant cross-sectional area. The physical motivation for this study came from a consideration of the dynamically important region beneath the overturning crest of a breaking gravity wave, in which high fluid-particle accelerations may develop (see Peregrine, Cokelet & McIver 1980).

In this context we have studied a wide variety of numerically generated breaking waves, in both deep and shallow water, and have found in each case that a certain section of the wave profile can be closely approximated by an ellipse of $\sqrt{3}$ aspect ratio. The region of this fit is demonstrated in figures 1–3. Figures 1 and 2 show two examples taken from a class of shallow-water breaking waves computed by New

† Present address: Institute of Oceanographic Sciences, Crossway, Taunton, Somerset TA1 2DW.

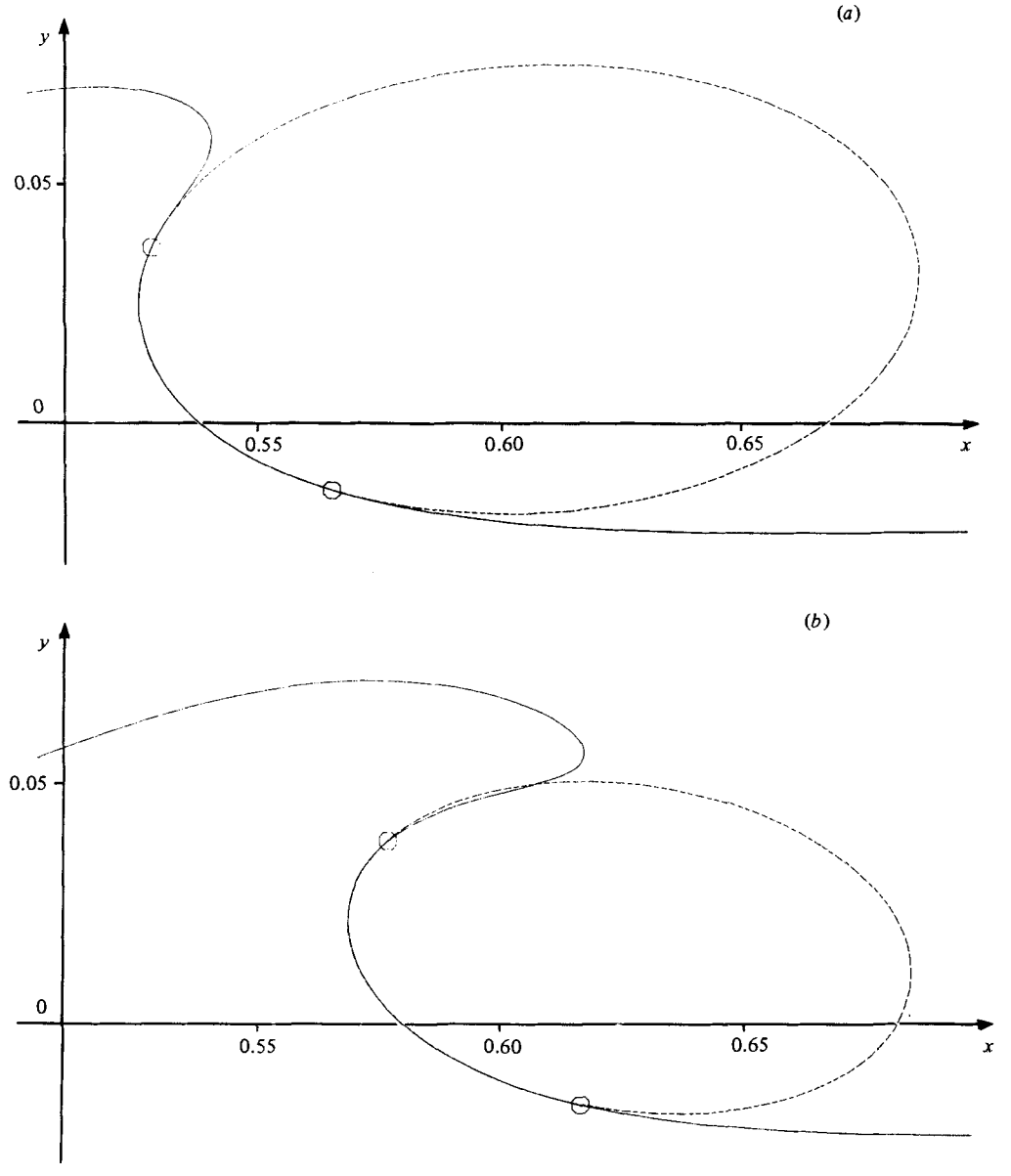

FIGURE 1 (*a*, *b*). For caption see facing page.

(1983). Starting from initial conditions representing a steep steadily progressing wave on depth $d_0 = 0.200$ (with wavelength $\lambda = 1$), the computations were then carried out on depths $d = 0.070$ (figure 1, labelled 'wave 1' in this paper) and $d = 0.132$ (figure 2, labelled 'wave 2'). Figure 3 shows the motion developing from an initial deep-water sine wave of large amplitude (labelled 'wave 3') due to McIver (1982, private communication). All these computations were performed with a high resolution, using 180 numerical particles in the free surface.† In each case, the section of the wave

† The calculation method for the deep-water wave was based on that of Longuet-Higgins & Cokelet (1976); for finite depth, a simple extension of this technique, described in New (1983), was employed.

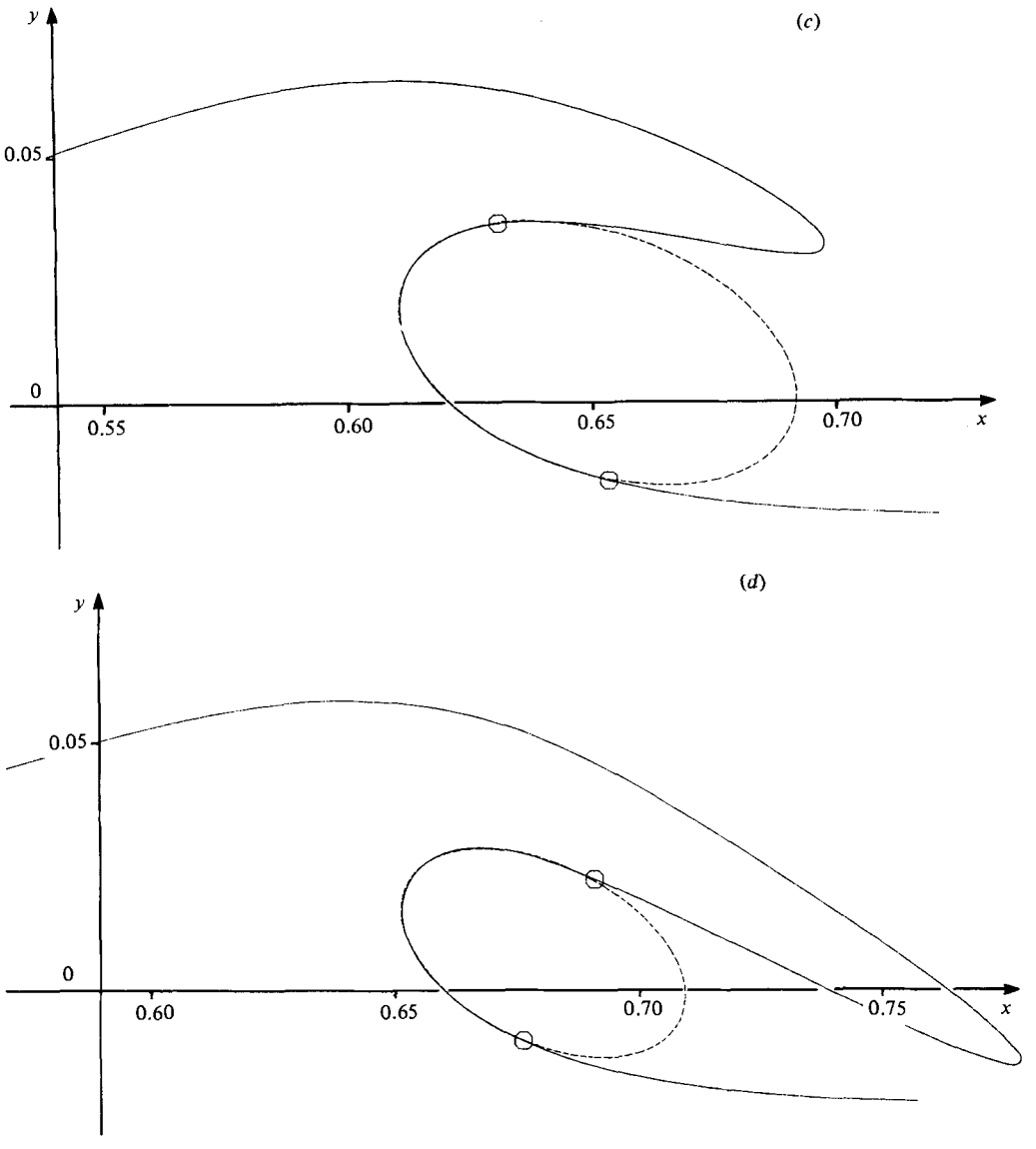

FIGURE 1. Fits of $\sqrt{3}$ aspect-ratio ellipses to wave 1. Horizontal and vertical axes are x and y respectively ($\lambda = 1$). —○——○—, wave profile, showing the extent of the fitted region; --------, ellipse. (*a*) $t = 1.150$; (*b*) 1.300; (*c*) 1.452; (*d*) 1.604.

profile fitted is indicated by the small circles, and throughout this region the coincidence is seen to be remarkable.

The ellipses shown in these figures are of aspect ratio $\sqrt{3}$ and were fitted numerically using a technique based on the method of least squares. If the aspect ratio itself is now also allowed to vary, producing an even closer fit to the same surface particles, its value typically becomes close to $\sqrt{3}$ when the wave is well developed, as shown in figure 4.

Apart from this numerical evidence, support is also provided by Miller (1976), who, in a study of the surf zone, has produced a number of good-quality photographs of plunger-generated breaking waves in the laboratory. Figures 5 and 6 of the present

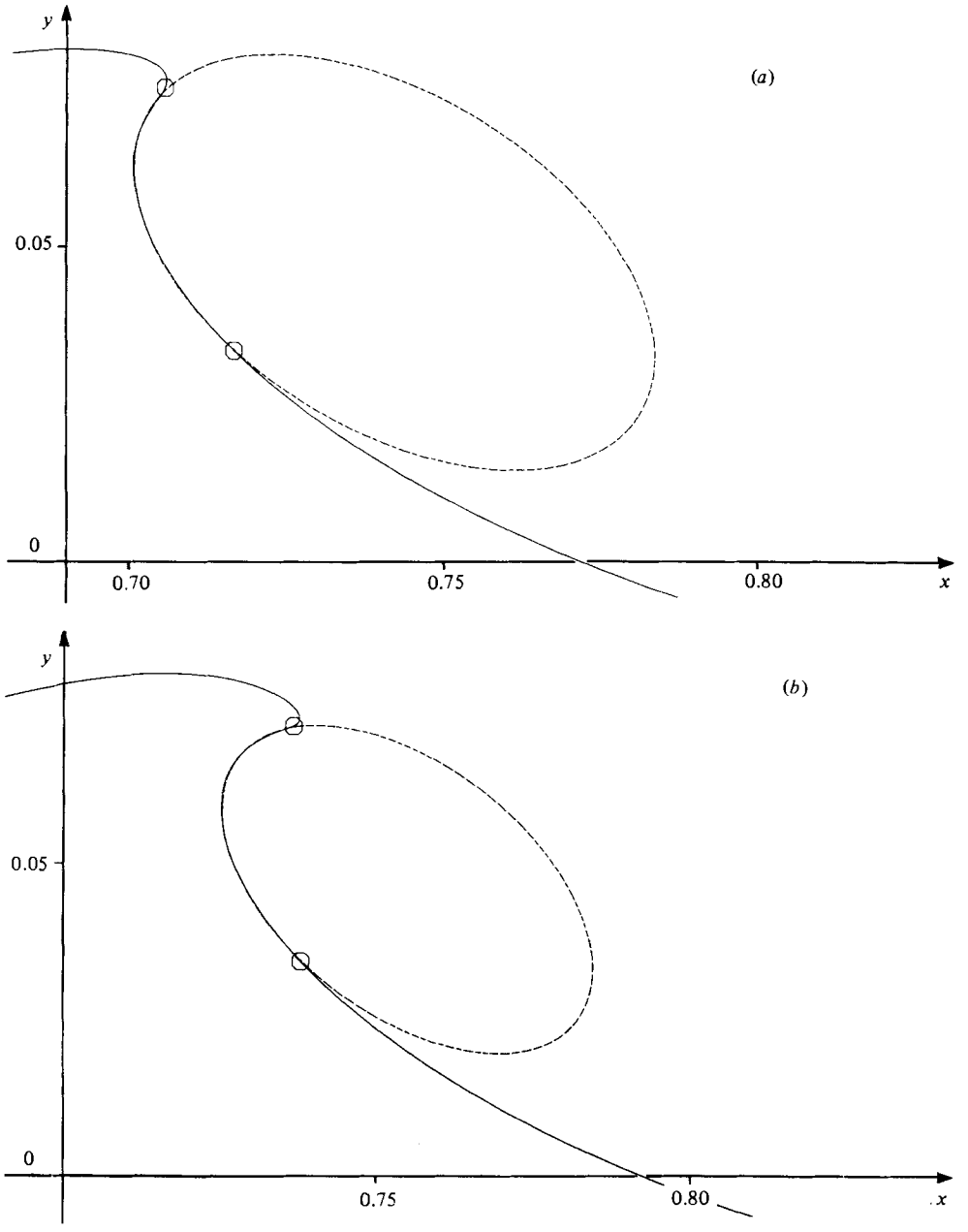

FIGURE 2(*a*, *b*). For caption see facing page.

paper show tracings from transparencies supplied by Miller, corresponding to figures 1 and 2 respectively of his paper, and again show closely fitting '$\sqrt{3}$-ellipses'. In particular, we see that the elliptical fit may even be a good approximation for some time after the 'touchdown' of the jet.

This intriguing phenomenon naturally prompts a search for an exact self-similar solution to the equations of motion in which the free surface takes on the form of an ellipse of time-constant aspect ratio. After considering a simple case in §2 in which the flow is contained between two concentric circles, §3 uses the formalism of John

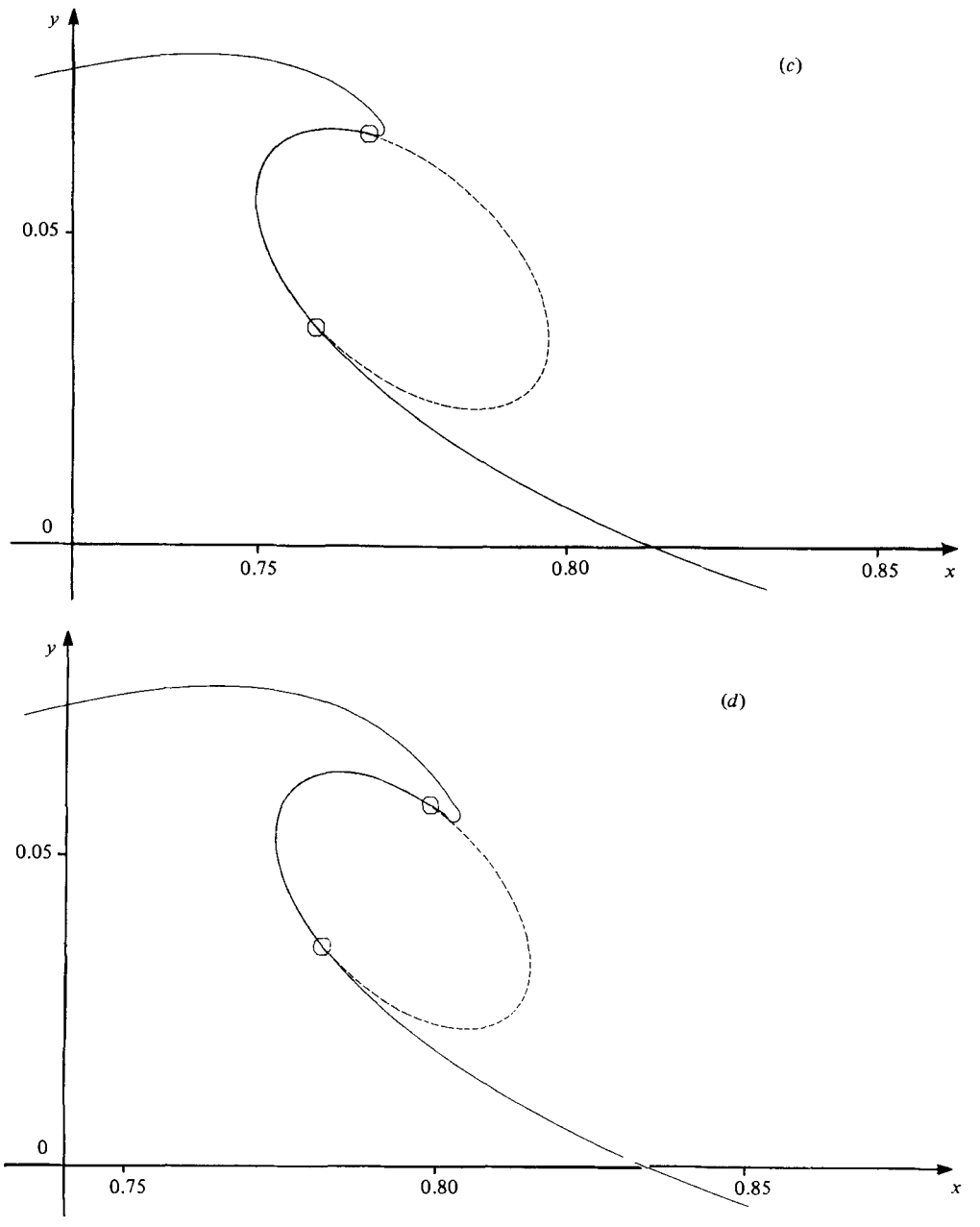

FIGURE 2. Fits of $\sqrt{3}$ aspect-ratio ellipses to wave 2. For legend see caption to figure 1. (*a*) $t = 1.620$; (*b*) 1.680; (*c*) 1.740; (*d*) 1.800.

(1953) to derive the ellipse solution. The aspect ratio is found to be constant but arbitrary in value.† Then in §4, wave 2 is fitted accurately by ellipses of $\sqrt{3}$ aspect ratio, and the relevance of the solution to breaking waves is discussed. Finally, §5 investigates a self-similar solution due to Longuet-Higgins (1981, 1982), in which the free surface is a parametric cubic curve.

† Thus the free-surface profiles are self-similar. The velocity and acceleration fields, however, are not!

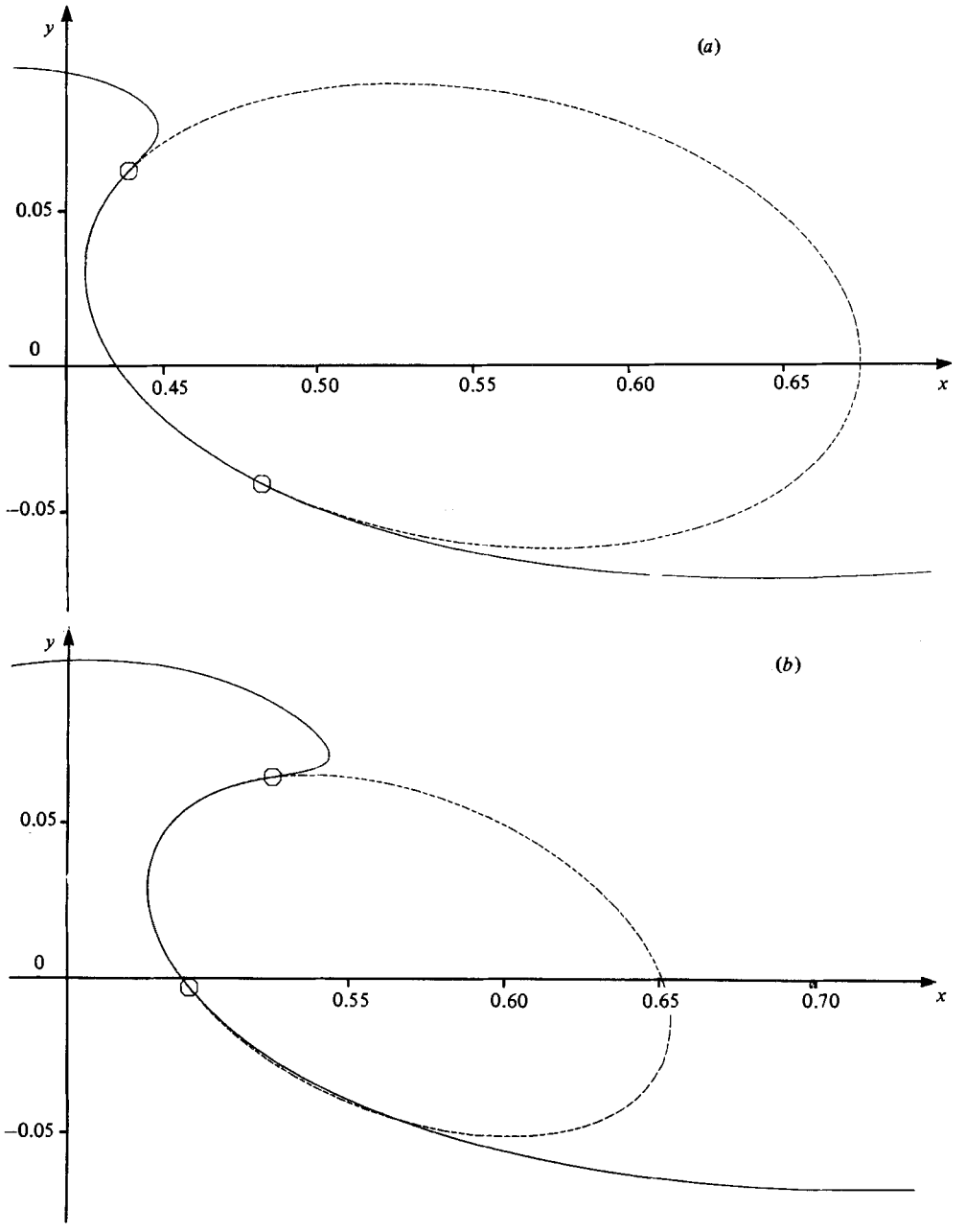

FIGURE 3 (*a*, *b*). For caption see facing page.

The class of elliptical free-surface flows developed in this paper adds to the body of known solutions of the exact equations of motion, and, although essentially in free fall, may be of especial relevance to many types of overturning gravity waves.

2. A preliminary investigation

Before embarking on a study of the class of elliptical flows, we first investigate a simple solution in which the fluid occupies the space between the two concentric circles $r = R(t)$ and $r = \bar{R}(t)$, where $\bar{R} > R$. We impose a pressure $p = p_0$ on the outer

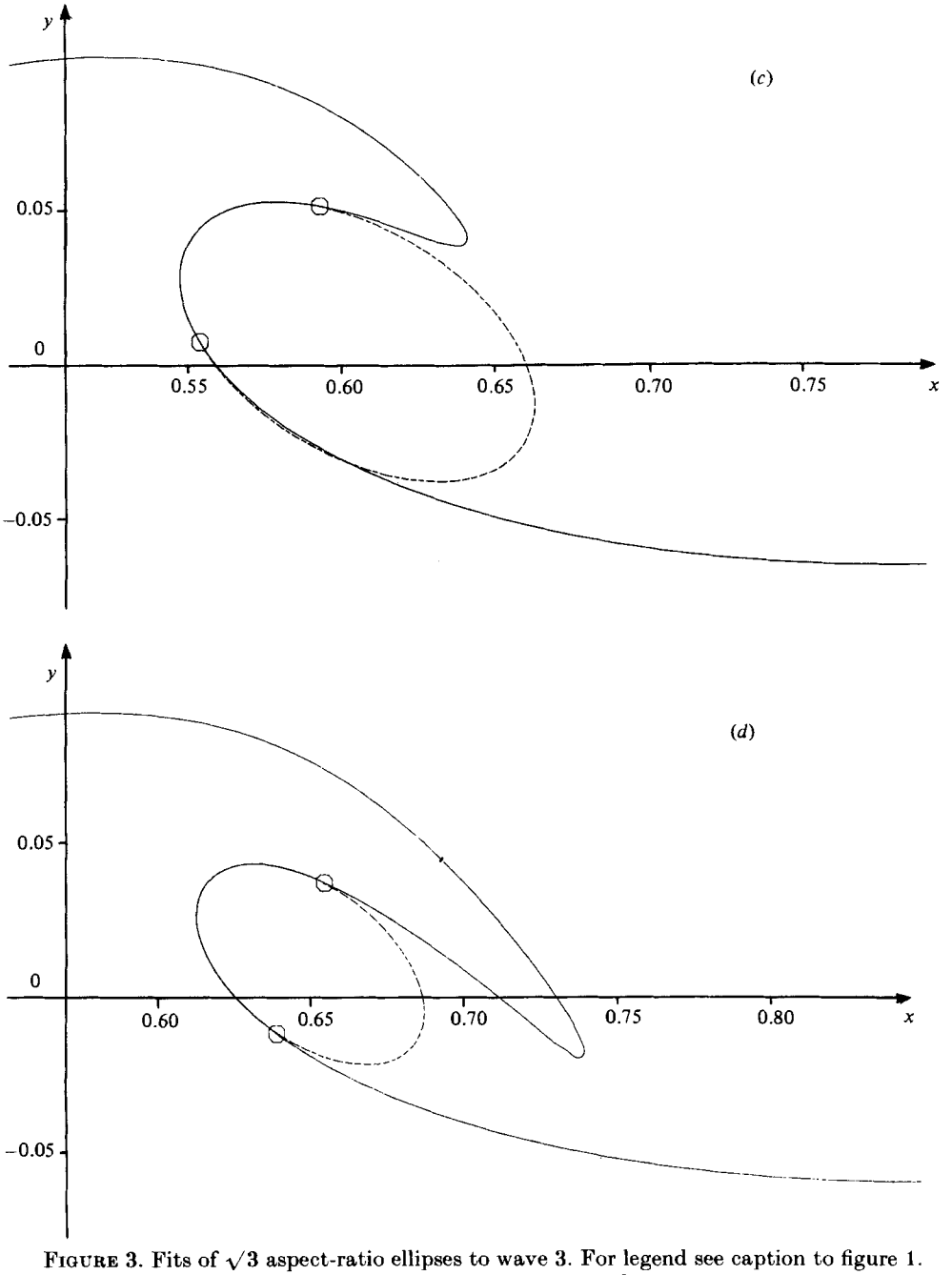

FIGURE 3. Fits of $\sqrt{3}$ aspect-ratio ellipses to wave 3. For legend see caption to figure 1. (*a*) $t = 1.086$; (*b*) 1.253; (*c*) 1.420; (*d*) 1.587.

surface, where p_0 is a constant. Since a fixed mass of air is trapped within the inner contour, we may take the pressure there to be $p = p_0/R^2(t)$. The symmetric situation is shown in figure 7.

Now suppose that the complex velocity potential is given as

$$W(z,t) \equiv \phi + \mathrm{i}\psi = f(t) + \mathrm{i}g(t) + (A(t) + iB(t)) \ln z, \tag{2.1}$$

which represents a simple singularity at the origin. Here $f(t)$, $g(t)$, $A(t)$ and $B(t)$ are

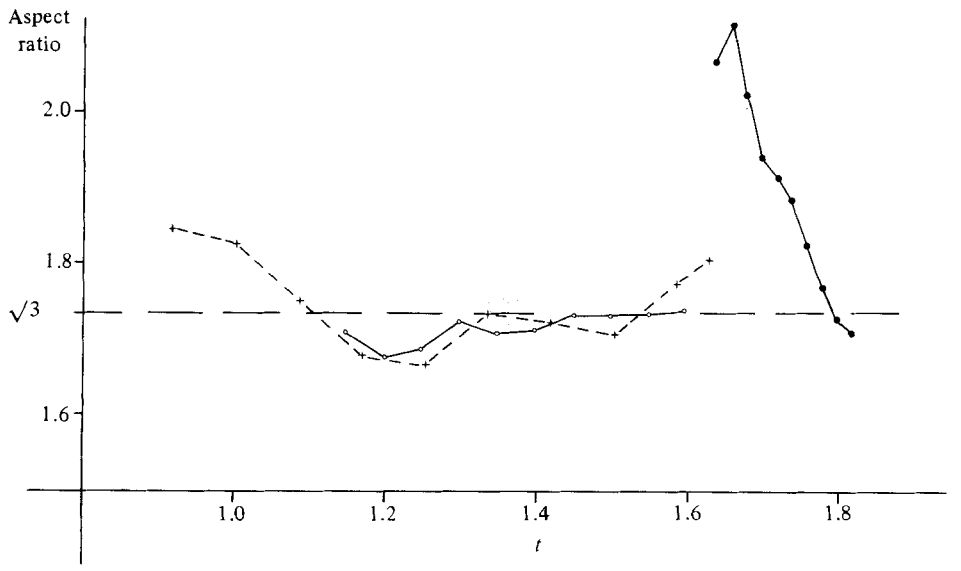

FIGURE 4. Time dependence of the aspect ratios of the 'best-fit' ellipses: —○——○—, wave 1; —●——●—, wave 2; – + – – – + –, wave 3.

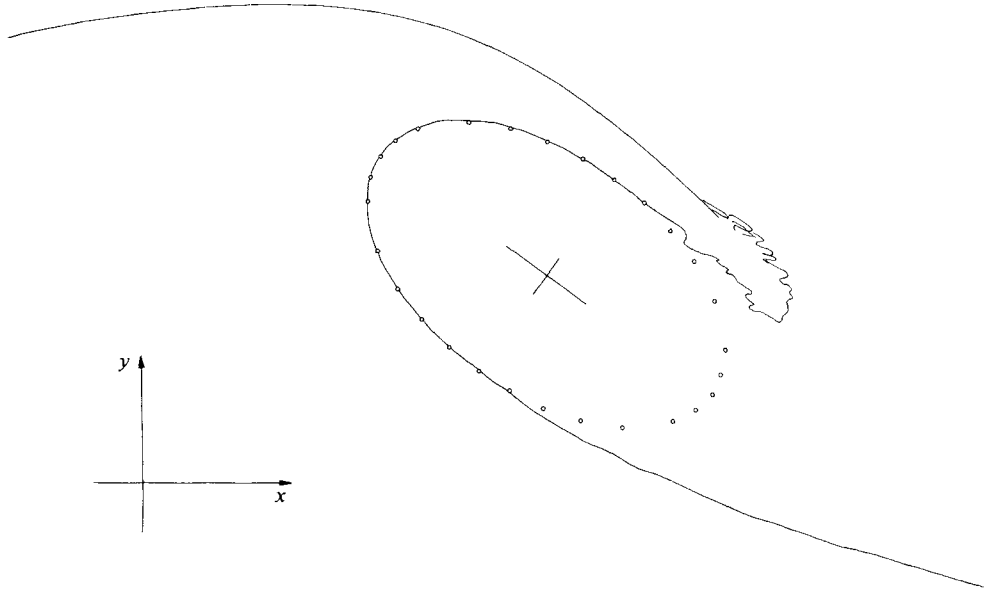

FIGURE 5. Laboratory wave of Miller (1976) and fitted ellipse of $\sqrt{3}$ aspect ratio.

real functions of the time. Neglecting gravity, the fluid pressure p then satisfies

$$-p \equiv \tfrac{1}{2}(W_t + W_t^*) + \tfrac{1}{2} W_z W_z^* = f_t + A_t \ln r - B_t \theta + \frac{A^2 + B^2}{2r^2}. \tag{2.2}$$

The kinematic boundary conditions on the two surfaces yield

$$A = R R_t = \bar{R} \bar{R}_t, \tag{2.3}$$

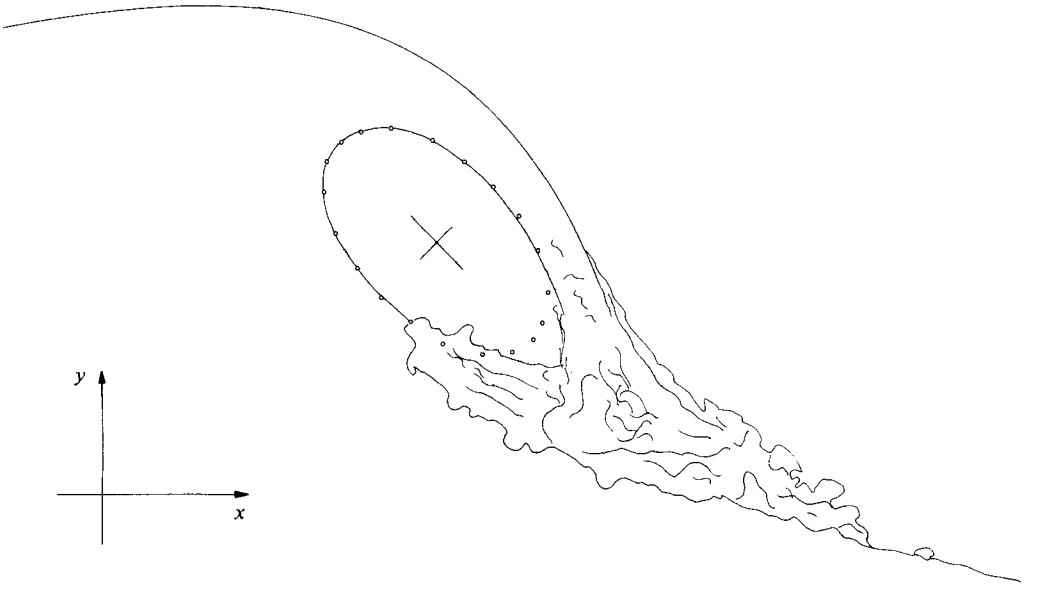

FIGURE 6. Laboratory wave of Miller (1976) and fitted ellipse of $\sqrt{3}$ aspect ratio.

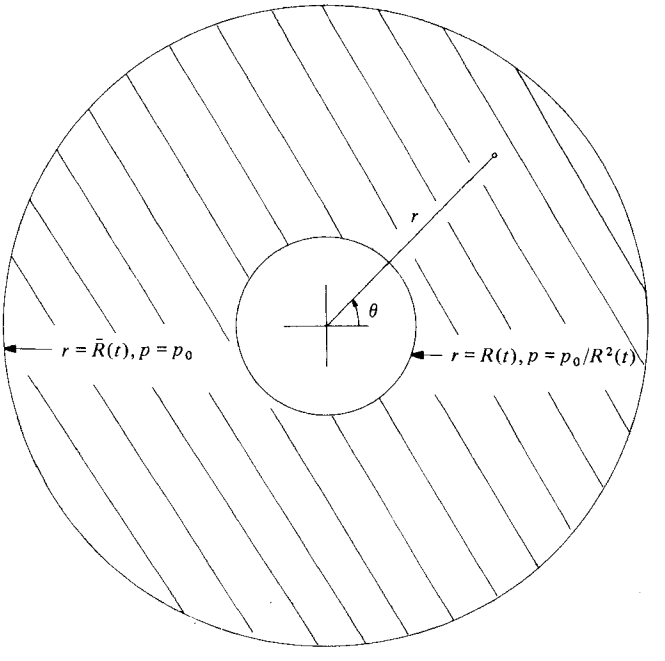

FIGURE 7. The fluid configuration of §2.

with first integral representing the conservation of mass:

$$\bar{R}^2 - R^2 = M, \tag{2.4}$$

where M is a positive constant. Also, we have

$$B = -\Gamma, \tag{2.5}$$

where $2\pi\Gamma$ is the constant circulation around any material curve.

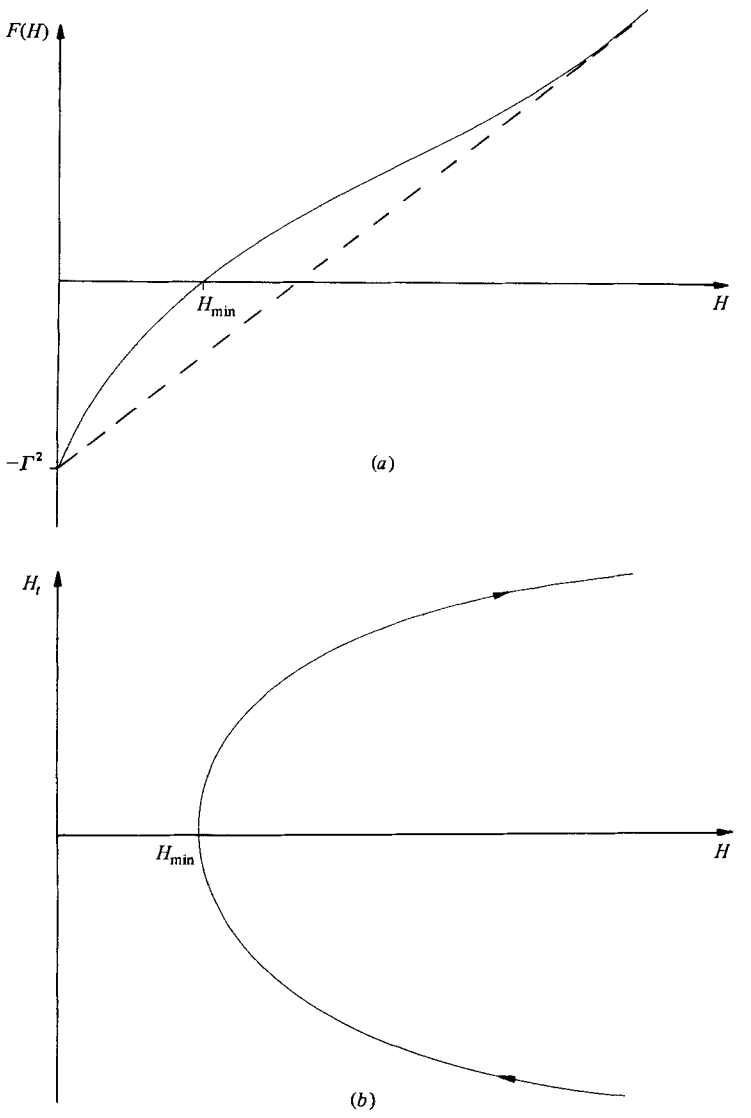

FIGURE 8. (a) The function $F(H)$ for the case $p_0 = 0$, see (2.7). ——, $F(H) = CH/M - \Gamma^2$. (b) Phase-plane trajectory of (2.7) for the case $p_0 = 0$.

Substituting these results into the dynamic conditions on the two surfaces and subtracting gives

$$\tfrac{1}{2}H_{tt}\ln\left(1+\frac{M}{H}\right)-\frac{1}{4}\frac{MH_t^2}{H(M+H)}=2p_0\left(\frac{1}{H}-1\right)+\frac{M\Gamma^2}{H(M+H)}, \tag{2.6}$$

where $H(t) \equiv R^2(t)$. Upon integration we then have

$$\tfrac{1}{4}H_t^2=\frac{C+2p_0(\ln H-H)}{\ln(1+M/H)}-\Gamma^2\equiv F(H), \text{ say}, \tag{2.7}$$

where C is an arbitrary constant of integration, and may be chosen (along with $H(0)$, p_0, M and Γ) to define the resulting motion.

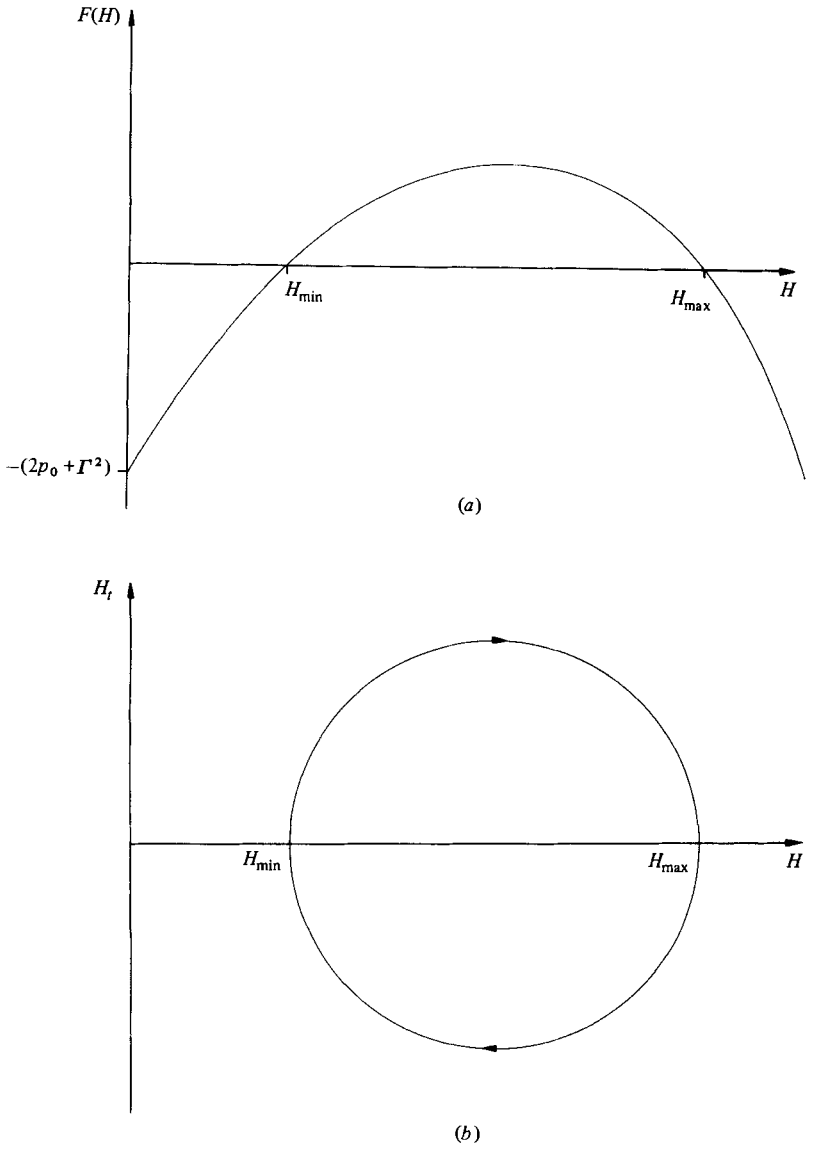

FIGURE 9. (*a*) The function $F(H)$ for the case $p_0 > 0$, see (2.7).
(*b*) Phase-plane trajectory of (2.7) for the case $p_0 > 0$.

We now consider the phase-plane portraits of (2.7) for two cases. Firstly, we suppose that the density of the air is negligible, and set $p_0 = 0$. Figure 8(*a*) shows $F(H)$ in this case, where C is positive. Clearly a solution only exists for H such that $F(H) \geqslant 0$, and the phase plane will be qualitatively as shown in figure 8(*b*). We see that $R(t)$ will in general contract to a minimum value ($H^{\frac{1}{2}}_{min}$) and then increase without limit. Only in the case of no circulation ($\Gamma = 0$) does the inner surface shrink to zero, since there is now no centrifugal acceleration to support the collapse.

If, however, we take $p_0 > 0$, the motion oscillates between two finite limits as indicated in figures 9(*a*,*b*). The solution typically 'bounces' at a larger minimum radius than in the case $p_0 = 0$ since the compression of the air inside the inner surface

produces an outward pressure gradient. Similarly, its rarefaction results in the finite maximum radius ($H^{\frac{1}{2}}_{\max}$).

It is shown by Greenhow (1983) that the ellipse solution of §3 possesses a second $p = 0$ surface which in the physical plane closely surrounds the elliptical contour. The fluid, for which $p \geqslant 0$, is then contained between these two boundaries. Thus the behaviour of the ellipse solution may be qualitatively similar to that of the simple flow of the present section, which provides physical insight into the nature of the problem.

3. Ellipse theory

Longuet-Higgins (1976, 1982) demonstrates the power of a semi-Lagrangian method due to John (1953) for deriving zero-gravity free-surface flows. This method is now employed to derive the elliptical solution.

Instead of considering the complex velocity potential $W \equiv \phi + \mathrm{i}\psi$ as a function of the position z and the time t, we now suppose that both W and z are functions of t and a further variable ω which at the free surface is real and Lagrangian (constant following a given fluid particle). Assuming gravity to act in the negative y-direction, John (1953) then shows that the dynamic condition of a pressure gradient normal to the free surface may be written as

$$z_{tt} + \mathrm{i}g = \mathrm{i}r(\omega, t)\, z_\omega, \tag{3.1}$$

where r is real at the free surface but otherwise artibrary. Further, a velocity potential consistent with the motion of the free surface is written as

$$W(\omega, t) = \int^{\omega} z_{\omega'}(\omega', t)\, z_t^*(\omega', t)\, \mathrm{d}\omega'. \tag{3.2}$$

We seek a free-fall solution ($g = 0$) of (3.1) in the form of an ellipse having a constant aspect ratio by supposing

$$z(\omega, t) = a(t)\, \mathrm{e}^{\mathrm{i}\chi(t)} \{\tfrac{1}{2}(1+\alpha)\, \mathrm{e}^{\mathrm{i}\theta(\omega, t)} + \tfrac{1}{2}(1-\alpha)\, \mathrm{e}^{-\mathrm{i}\theta(\omega, t)}\}. \tag{3.3}$$

Here $a(t)$ represents the length of the major axis ($\theta = 0$), inclined at an angle $\chi(t)$ to the horizontal x-direction, $\theta(\omega, t)$ is the fluid-particle orientation relative to the major axis, and the aspect ratio is $1/\alpha$. The neglect of gravity may be to some extent justified, since for a well-formed breaking wave, the jet tip quickly attains a state of free fall, and the fluid accelerations in the 'ellipse' region may be as high as $4g$ or $5g$.

Substituting (3.3) into (3.1) and equating the coefficients of $\exp \mathrm{i}(\chi \pm \theta)$ separately to zero gives two complex equations. The real parts are

$$a_{tt} - a(\chi_t \pm \theta_t)^2 = \mp r\theta_\omega a, \tag{3.4}$$

and the imaginary parts:

$$2a_t(\chi_t \pm \theta_t) + a(\chi_{tt} \pm \theta_{tt}) = 0. \tag{3.5}$$

At this point we remark that the aspect ratio has vanished from the problem and is thus arbitrary! Adding and subtracting first (3.4) and then (3.5) yields

$$a_{tt} - a(\chi_t^2 + \theta_t^2) = 0, \tag{3.6a}$$

$$2\chi_t \theta_t = r\theta_\omega, \tag{3.6b}$$

$$2a_t \chi_t + a\chi_{tt} = 0, \tag{3.6c}$$

$$2a_t \theta_t + a\theta_{tt} = 0. \tag{3.6d}$$

Now we see from (3.6a) that θ_t is a function of t alone and from (3.6b) that $r\theta_\omega$ is hence also a function of only t. Thus the ω-variation in θ is arbitrary and depends on the choice of the function $r(\omega, t)$. This in turn implies that the branch points of the solution, as given by the vanishing of z_ω (or θ_ω) when not annulled by a zero of $(W_z)_\omega$, may be specified by the infinities of $r(\omega, t)$. For any physically realizable flow these must be contained outside the fluid domain.

Integrating (3.6c,d) gives

$$a^2\chi_t = B, \tag{3.7a}$$

$$a^2\theta_t = AB, \tag{3.7b}$$

where A and B are real constants. Typically, from numerical comparisons of waves breaking from left to right, we observe that the fitted ellipse rotates clockwise, giving $B < 0$, and that fluid particles themselves also rotate clockwise relative to the ellipse, so that $A > 0$. From (3.7) we conclude that

$$\theta(\omega, t) = A\chi(t) + G(\omega), \tag{3.8}$$

where $G(\omega)$ is arbitrary, so that any given fluid particle rotates relative to the ellipse exactly A times as fast as the ellipse itself rotates. This is investigated further in §4.

Substituting (3.7) into (3.6a) and integrating once yields

$$a_t^2 = (Ca^2 - B^2(1+A^2))/a^2, \tag{3.9}$$

where C is a constant of integration which is necessarily positive. Thus $a(t)$ has a minimum value of $a_{\min} = (B^2(1+A^2)/C)^{\frac{1}{2}}$ attained when $a_t = 0$, at time $t = t_0$ say. The ellipse can only contract to zero when $B = 0$. In this case there is no rotation and the analogy with §2 is apparent.

Integrating (3.9) again yields

$$a^2(t) = C(t-t_0)^2 + a_{\min}^2, \tag{3.10}$$

and finally from (3.7a) we obtain

$$\chi(t) = \chi_0 + (1+A^2)^{-\frac{1}{2}} \arctan \frac{C^{\frac{1}{2}}(t_0 - t)}{a_{\min}}, \tag{3.11}$$

where $\chi_0 \equiv \chi(t_0)$ is another constant of the motion. Typically, for numerically-generated breaking waves, $t < t_0$, so that both $a(t)$ and $\chi(t)$ decrease as t increases.

4. An elliptical fit

Because the region of the elliptical free surface does not occupy a large portion of the complete wavelength it is only possible to obtain fits of satisfactory accuracy if the numerical wave profile contains a large number of computational particles. Hence ellipses of $\sqrt{3}$ aspect ratio were fitted in detail to the three 180-point examples waves 1, 2 and 3, a number of representative times being chosen for each to cover the period of jet ejection. For each profile, using a technique based on the method of least squares, an ellipse was fitted to a certain number (typically 20) of successive surface particles, which were chosen to produce the most accurate fit. The region of the free surface approximated in this way is indicated in figures 1–3. The results from these three examples are found to be similar in character, and systematic differences with the ellipse theory arise. For this reason, only the fit to wave 2 is discussed.

Figure 10 shows the time variation of $a(t)$ and $\chi(t)$ resulting from the numerical fitting, and also theoretical curves, (3.10) and (3.11) respectively, which provide a

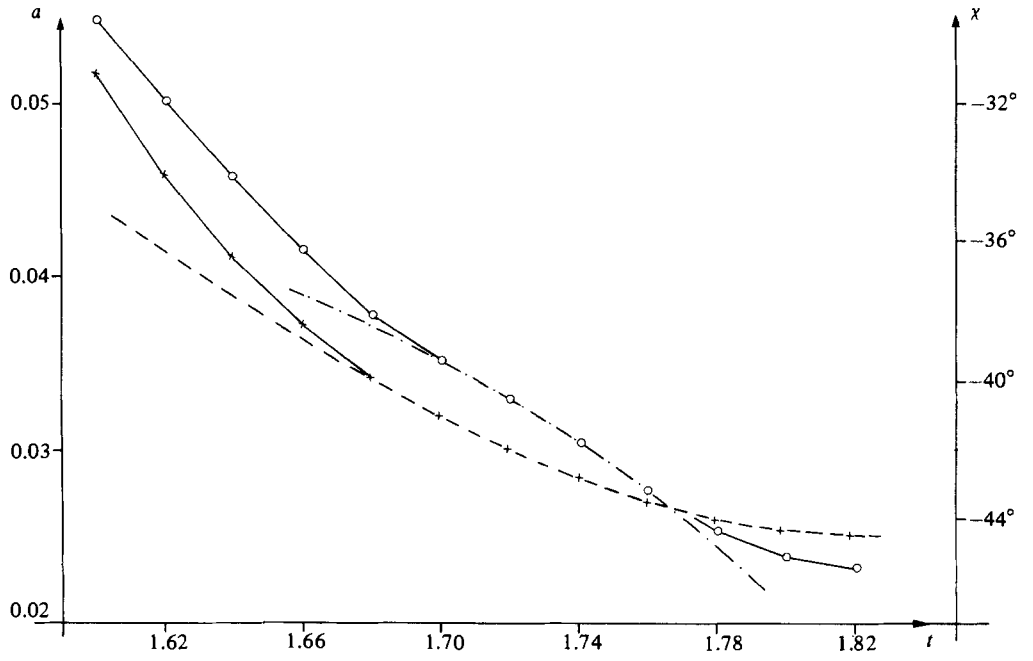

FIGURE 10. Time dependence of $a(t)$ and $\chi(t)$: +, values of $a(t)$ from numerical fitting of $\sqrt{3}$ aspect-ratio ellipses to wave 2; ○, values of $\chi(t)$ from numerical fitting of $\sqrt{3}$ aspect-ratio ellipses to wave 2; – – – –, (3.10) with parameters as in (4.1); –·–·–·–, (3.11) with parameters as in (4.2).

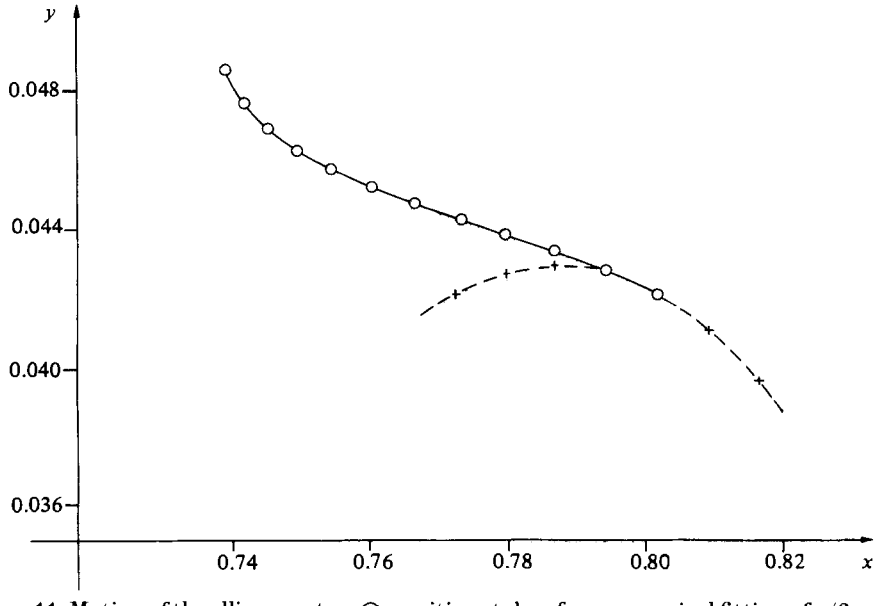

FIGURE 11. Motion of the ellipse centre: ○, positions taken from numerical fitting of $\sqrt{3}$ aspect-ratio ellipses to wave 2; – + – – – – + –, a free-fall trajectory.

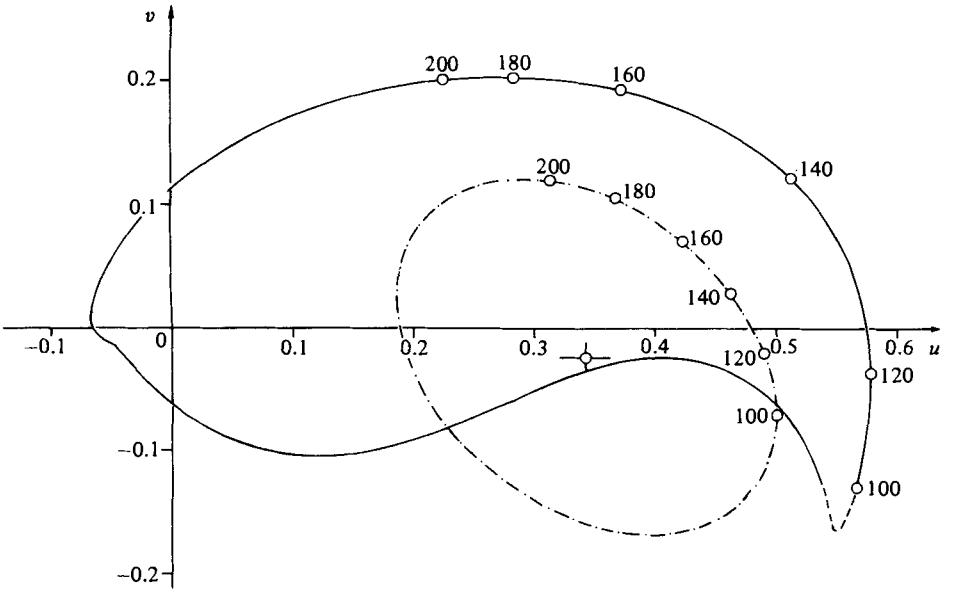

FIGURE 12. Hodograph comparison with ellipse theory: ——, contour of numerical velocities, taken from wave 2 at $t = 1.76$; – – – – –, region of doubtful accuracy in the numerical profile; – · – · – · –, ellipse theory. Both curves are labelled with values of the fluid-particle orientation relative to the horizontal space axis, taken from the ellipse centre.

satisfactory approximation. In this way the parameters needed to specify the ellipse solution are found to be

$$C = 0.02584, \quad t_0 = 1.8235, \quad a_{\min} = 0.0248, \tag{4.1}$$

from the theoretical curve for $a(t)$, and

$$\chi_0 = -48.5, \quad A = 4.13, \tag{4.2}$$

from the curve for $\chi(t)$ (note that $B = -9.38 \times 10^{-4}$ is determined from the value of $a_{\min}$). We see that the agreement in this figure is good at least between $t = 1.70$ and $t = 1.76$. Before $t = 1.70$ the elliptical profile may not be sufficiently developed to conform to the theoretical curves, and for $t > 1.76$ the discrepancies could be caused by the numerical solution losing accuracy, since breakdown of the method occurs at $t = 1.835$.

It should be noted that the ellipse theory of §3 is developed for a reference frame in which gravity is neglected, so that the solution should be in a state of free fall. The path of the ellipse centre in the present example is shown in figure 11, and it seems possible that the motion may be developing along the indicated free-fall trajectory. However, similar behaviour is not found for waves 1 and 3. This may be due in part to the proximity of the wave trough to the ellipse region in these examples (see figures 1 and 3), preventing the ellipse from falling in the vertical direction.

In spite of this difficulty, it is still worthwhile to make a comparison of the fluid-particle velocities predicted from the ellipse theory (with parameters as given in (4.1) and (4.2)) with the numerical values. Figure 12 shows a typical hodograph comparison (at $t = 1.76$) in which the labelling on each contour represents the particle orientation relative to the horizontal space axis ($\theta^* \equiv \theta + \chi$ degrees). The origin of the ellipse contour is at $(u, v) = (0.341, -0.024)$ corresponding to the instantaneous velocity of

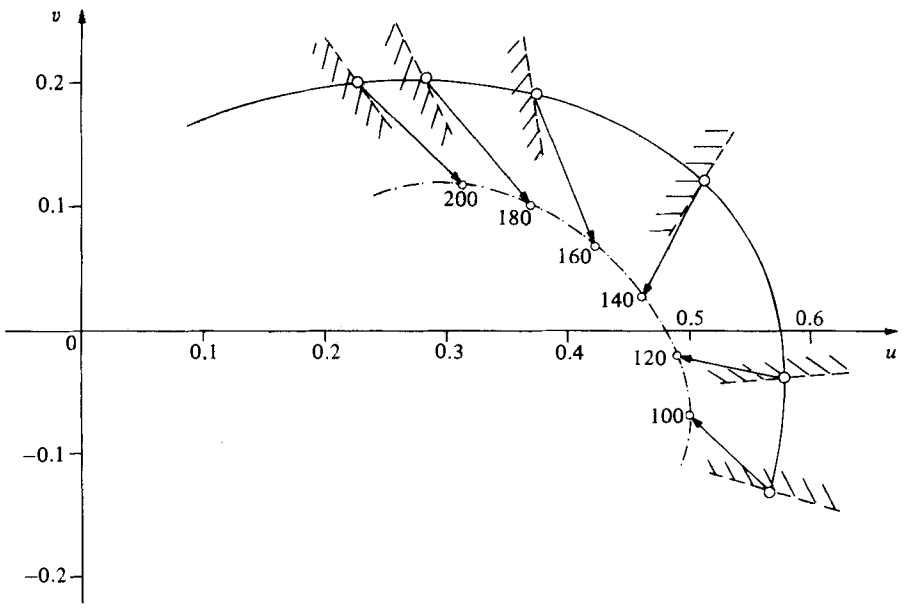

FIGURE 13. Differences between the numerical velocities and those predicted by the ellipse theory: ////////, indication of the free surface, with the fluid shown shaded. (See also caption to figure 12 for legend.)

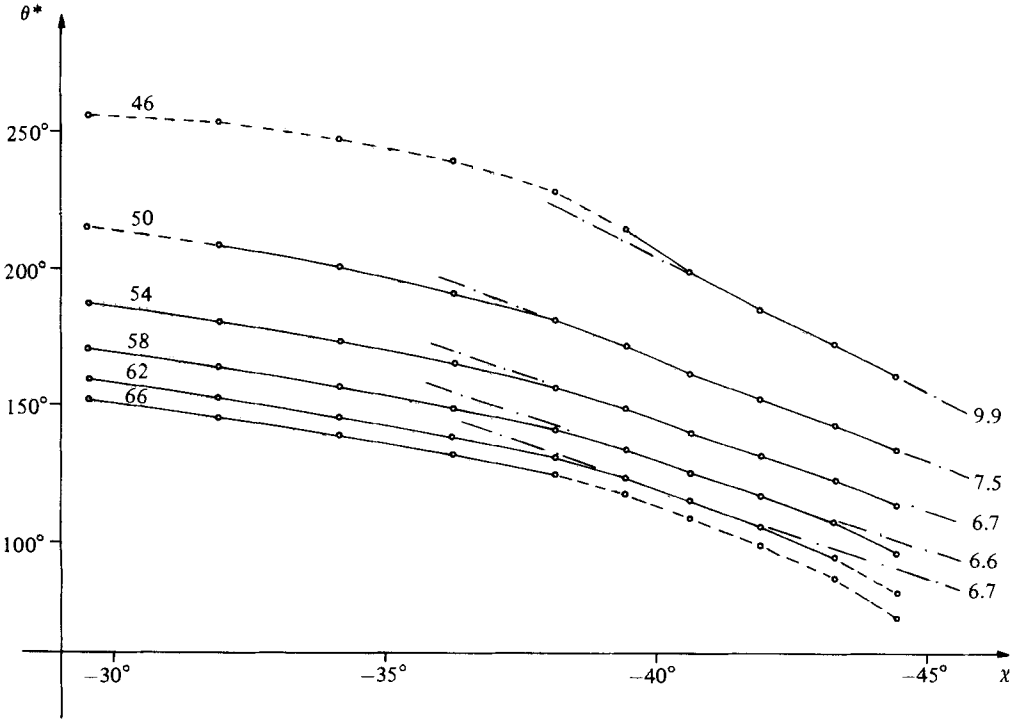

FIGURE 14. Particle rotation around the ellipse (θ^* and χ: see text): O——O, fluid particle contained in the region of the wave profile fitted by the ellipse; O– – – –O, fluid particle not within this region (the numbers of the computational particles followed are shown at the left-hand side of each trajectory); –·–·–, straight-line segments, with gradients indicated at the right-hand side.

the ellipse centre. We see that over the region of the elliptical fit ($100° < \theta^* < 200°$) not only are the shapes of the two curves similar, but also the angular dependence is well described. Figure 13 shows that the velocity differences are roughly in the direction of the tangent to the free surface, so that the systematic discrepancies imply an underestimation by the theory of the rotation rate of the fluid particles around the ellipse.

To investigate this aspect further we have plotted, in figure 14, θ^* against χ for various numbered computational particles as they travel through the elliptical region. From the theory we have

$$\theta^*(\omega, t) = (A+1)\,\chi(t) + G(\omega), \tag{4.3}$$

so that the trajectory of each particle should be a straight line with slope $A+1 = 5.13$. We see that, when the ellipse is 'well-formed' (i.e. $t > 1.68$), the particle paths are indeed almost linear, but with slopes varying from about 6.5 to 10.0, as we might expect. It would almost seem that the fluid particles are rotating too quickly to remain on the elliptical profile, being thrown outwards into the jet under centrifugal action. This figure indicates that we need to find a solution in which $A \equiv A(\omega)$ rather than an absolute constant.

The elliptical flow does not of course model the discontinuity in velocity where the tip of the jet meets the forward face of the wave, and, in view of the differences between the predicted and computed velocities, a presentation of the accelerations is not thought to be worthwhile. Although the accelerations as given by the theory are qualitatively correct over the region fitted by the ellipse, pointing outwards from the fluid, they are significantly smaller than the computed values. In any case we do not expect the predicted accelerations, symmetrical about the ellipse centre, to be a good model for the asymmetric situation in a breaking wave.

5. A cubic description

We have seen that the ellipse solution needs certain modification if it is to accurately describe the flow beneath the overturning crest of a breaking gravity wave. An alternative solution due to Longuet-Higgins (1981, 1982) is now investigated, in which the free surface takes the form of a parametric cubic curve.

Using the same formalism as in §3, Longuet-Higgins shows that

$$z(\omega, \tau) = \mathrm{i}\tau\omega^3 + 3\tau^2\omega^2 - 2\mathrm{i}\tau^3\omega - \tfrac{1}{3}\tau^4, \tag{5.1a}$$

$$r(\omega, \tau) = -\frac{2}{\tau}, \tag{5.1b}$$

is a free-fall solution of (3.1). This is in fact the flow $z = -P_3$ of these papers, and, to distinguish it from the 'real' (computed) time of §§3 and 4, we take τ as the new time variable. The free surface is now described in the self-similar form

$$\frac{x}{\tau^4} = 3\mu^2 - \tfrac{1}{3}, \tag{5.2a}$$

$$\frac{y}{\tau^4} = \mu^3 - 2\mu, \tag{5.2b}$$

where $\mu \equiv \omega/\tau$ is a real parameter. Here we take τ as negative and increasing to zero so that the flow is contracting. The fluid region corresponds to the exterior of the above cubic curve, which is shown in figure 15. (Here we have taken $|\tau| = 0.3452$ to give an appropriate scaling for a later comparison.)

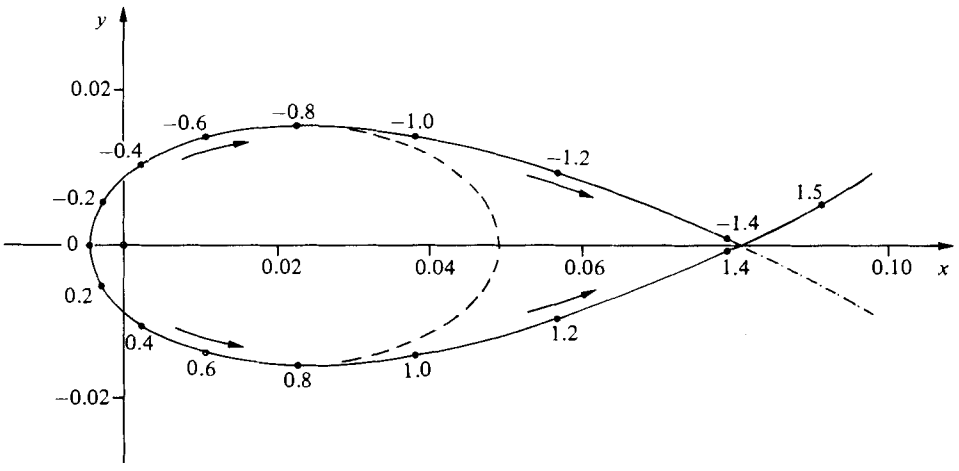

FIGURE 15. Self-similar cubic solution (5.2); the curve is labelled with values of μ (see text): $\longrightarrow$ indicates particle motion; ----, a $\sqrt{3}$ aspect-ratio ellipse.

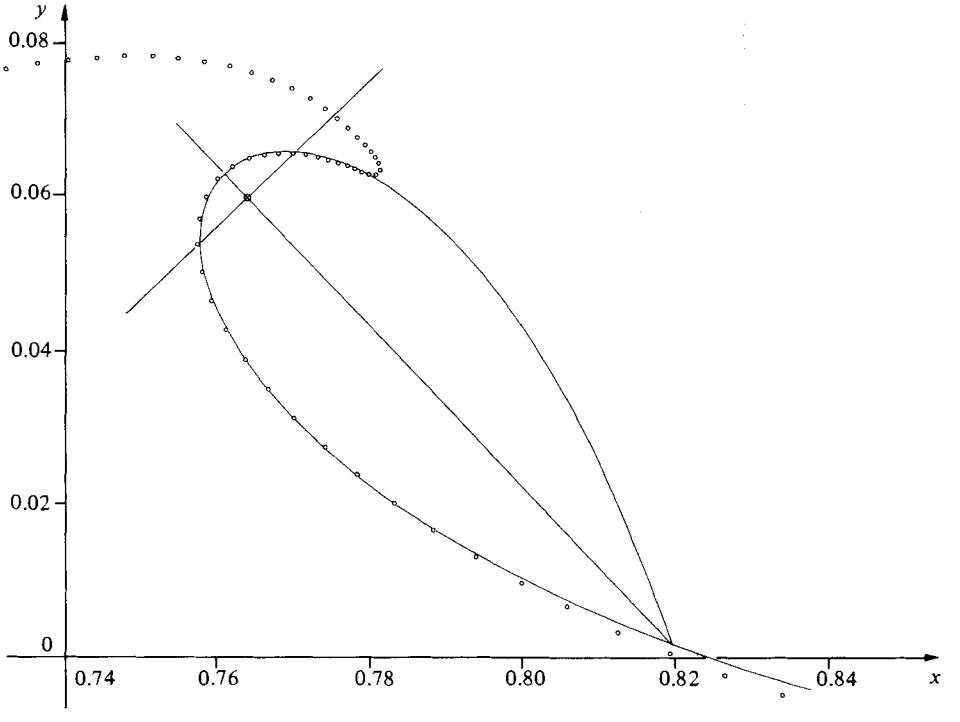

FIGURE 16. A profile comparison: ——, (5.2) with $|\tau| = 0.3452$ and axes rotated through $-46.5°$; ○, computational particles in wave 2 at $t = 1.76$.

Also shown in this diagram is an example of a $\sqrt{3}$ aspect-ratio ellipse which is practically indistinguishable from the present cubic curve for a large range of μ ($|\mu| \leqslant 0.8$). This agreement clearly means that any portion of the wave profile which is closely fitted by the ellipse may also be approximated by the cubic. A typical example, taken from wave 2 at time $t = 1.76$, is given as figure 16, and we note that the cubic seems to provide a close fit for some considerable distance along the forward face of the wave.

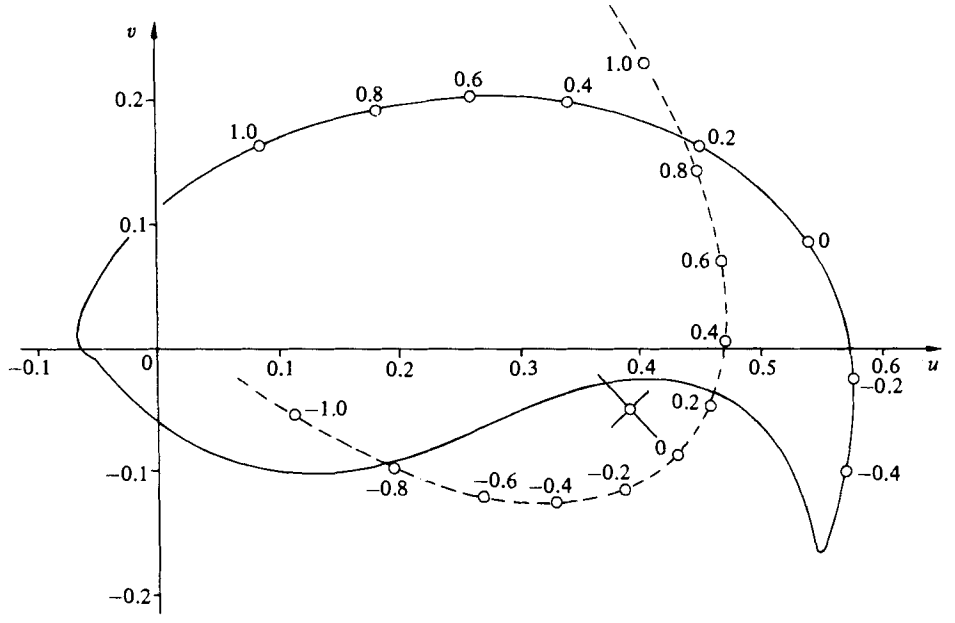

FIGURE 17. Hodograph comparison with the cubic solution of (5.1): ——, contour of numerical velocities, taken from wave 2 at $t = 1.76$; – – – –, velocities predicted from (5.1) (see text). Both curves are labelled with values of μ.

However, the corresponding hodograph comparison (figure 17) indicates that the velocities are not so well given by the cubic. The axes of the present solution are rotated through $-46.5°$ and translated to $(u, v) = (0.39, -0.05)$ to allow for the instantaneous orientation and velocity of the profile fit. Over the fitted region (say $-0.5 < \mu < 1.1$) the only similarity between the two curves is that the velocity vector rotates clockwise as μ decreases: the contours are dissimilar in shape and the μ-dependence is not well given. This diagram should be compared with figure 12, the velocities predicted from the ellipse theory, which seems to give a more realistic representation.

One notable difference between the two solutions is that the ellipse rotates, whereas the cubic solution P_3 (by itself) does not. The major axis of the fitted ellipse in figures 1–3 rotates (clockwise) through angles of 30°, 13° and 27° respectively, and for waves 1 and 3 McIver (1982) finds that a numerically fitted cubic rotates through 22° in each case during the same time intervals. Similarly, in fitting the cubic solution P_3 to numerical data, Longuet-Higgins (1981, 1982) obtains a rotation of 10°. To account for this rotation, which is small compared with the rotation of typical fluid particles, Longuet-Higgins suggests adding to P_3 a small fraction of a second cubic solution given by

$$Q_3 = -\mathrm{i}\omega^3 - 6\tau \ln|\tau|\omega^2 + 12\mathrm{i}\tau^2(\ln|\tau| - \tfrac{3}{2})\omega + 4\tau^3(\ln|\tau| - \tfrac{7}{3}), \tag{5.3}$$

so that

$$z = -P_3 - \mathrm{i}\eta Q_3, \tag{5.4}$$

where η is a small real constant. He finds that when $\eta = 0.1$ the axes of the cubic do indeed rotate through approximately the required angle.

The solution P_3 by itself possesses no systematic fluid-particle circulation: as τ increases to zero, the μ-value for any fixed fluid particle must increase to infinity without changing sign, so that the particles rotate away from the vertex ($\mu = 0$) as shown in figure 15. However, it appears that the addition of Q_3 to the solution

produces a modification of the velocity field which, for typical values of τ, is proportionally much larger than the constant η and which does indeed give a systematic rotation, thus improving the description of the fluid flow. This is an essential aspect of the problem which, as we have seen in §4, must be well modelled by any proposed solution: even though all the particles rotate in the correct direction in the ellipse theory (clockwise), the underestimation of the magnitude of this effect is thought to be the primary cause of the velocity differences.

6. Discussion

In this paper we show that a certain region of the surface profile beneath the overturning crest of a breaking gravity wave may be well approximated by an ellipse which has a time-constant aspect ratio equal to $\sqrt{3}$. Using the method of John (1953), the power of which is demonstrated by Longuet-Higgins (1976), we derive an elliptical solution to the equations of motion which models qualitatively certain essential features of the fluid flow seen in numerically-generated waves. Although the ellipse centre should move in a free-fall trajectory, its precise motion cannot be determined from the present theory, which allows an arbitrary constant velocity to be added to the solution corresponding to a change of reference frame. This is made physically plausible when we consider that the ellipse is only a local solution which may be influenced by the rest of the wave.

A similar flow due to Longuet-Higgins (1981, 1982), in which the free surface is a parametric cubic curve, is also investigated. Although the wave profile beneath the overturning crest is again well approximated, the fluid-particle motion is found to be poorly described unless a second cubic solution is added. (Further improvements to the description of the flow-field are suggested by Greenhow (1983)!)

The present ellipse theory shows that the solution may assume an arbitrary but time-constant aspect ratio. That all breaking waves so far investigated, in both deep and shallow water, possess a $\sqrt{3}$ aspect-ratio ellipse seems quite remarkable. Presumably this very definite shape is 'forced' in some way both by the flow into the elliptical region from beneath the forward face of the wave, and also by the imposed pressure gradient from the 'support region' on the rear face (see Peregrine *et al.* 1980). This gives us hope that there may be some general underlying structure common to all overturning waves, and is an incentive for further work to be carried out.

The author wishes to thank Dr D. H. Peregrine for his helpful comments and discussions and Dr P. McIver for providing the deep-water wave and data from numerical fits of the cubic curve. Thanks are also due to Prof. M. S. Longuet-Higgins for suggesting improvements to the original manuscript.

The financial support of the Natural Environment Research Council is gratefully acknowledged.

REFERENCES

CRAPPER, G. D. 1957 An exact solution for progressive capillary waves of arbitrary amplitude. *J. Fluid Mech.* **2**, 532–540.

GREENHOW, M. 1983 Free-surface flows related to breaking waves (unpublished manuscript).

JOHN, F. 1953 Two-dimensional potential flows with a free boundary. *Communs Pure Appl. Maths* **6**, 497–503.

LAMB, H. 1932 *Hydrodynamics*, 6th edn. Cambridge University Press.

LONGUET-HIGGINS, M. S. 1972 A class of exact, time-dependent, free-surface flows. *J. Fluid Mech.* **55**, 529–543.

LONGUET-HIGGINS, M. S. 1976 Self-similar, time-dependent flows with a free surface. *J. Fluid Mech.* **73**, 603–620.

LONGUET-HIGGINS, M. S. 1980 On the forming of sharp corners at a free surface. *Proc. R. Soc. Lond.* A **371**, 453–478.

LONGUET-HIGGINS, M. S. 1981 A parametric flow for breaking waves. In *Proc. Intl Symp. on Hydrodynamics in Ocean Engineering, Trondheim, Norway*, vol. 1, pp. 121–135. University of Trondheim.

LONGUET-HIGGINS, M. S. 1982 Parametric solutions for breaking waves. *J. Fluid Mech.* **121**, 403–424.

LONGUET-HIGGINS, M. S. & COKELET, E. D. 1976 The deformation of steep surface waves on water. I. A numerical method of computation. *Proc. R. Soc. Lond.* **A350**, 1–26.

MILLER, R. L. 1976 Role of vortices in surf zone prediction: sedimentation and wave forces. In *Beach and Nearshore Sedimentation* (ed. R. A. Davis & R. I. Ethington), pp. 92–114. Soc. Econ. Paleontologists and Mineralogists Spec. Publ. 24.

NEW, A. L. 1983 On the breaking of water waves. Ph.D. thesis, University of Bristol.

PEREGRINE, D. H., COKELET, E. D. & MCIVER, P. 1980 The fluid mechanics of waves approaching breaking. In *Proc. 17th Conf. Coastal Engng, Sydney*, pp. 512–528. A.S.C.E.